

Crystal Structures of Solid Solutions of a Symmetrical Ketone/*n*-Alkane Binary System

Keiko Nakasone*[1] and Norio Nemoto[2]

[1]Department of Physics and Earth Sciences, Faculty of Science, University of the Ryukyus, Nishihara, Okinawa 903-0213

[2]Department of Molecular and Material Sciences, IGSES, Kyushu University, Hakozaki, Fukuoka 812-8581

Received October 12, 2006; E-mail: b984022@sci.u-ryukyu.ac.jp

An X-ray diffraction study on the crystal structures of binary mixtures of very pure long-chain symmetrical ketone (K39) and *n*-alkane (C39) with an odd carbon number of 39 is presented. When the samples were prepared with the solution-crystallization method, which form two different types of solid solutions for the molar fraction (f_m) of K39 above and below $f_{m,c} = 0.204$. From composition and temperature dependencies of a long period (L) and two subcell lengths (a_s and b_s) determined from (00ℓ), (200), and (110) reflections, respectively, we show that nearly the same crystal structure as that of pure C39 is maintained for the solid solutions in regime S_1 where $f_m < f_{m,c}$, while K39 dominantly affects the crystal structures at room temperature in regime S_2 where $f_m > f_{m,c}$. When temperature was raised above the solidus line of the phase diagram in the S_2 regime, recrystallization occurred to form a solid solution very rich in the K39 component in the liquid–solid solution coexisting phase before final melting of K39. The solid–solid phase transition behaviors and resulting chain packing in the S_1 regime are discussed in relation to anomalous anisotropy of linear thermal expansion coefficients along two lattice directions.

Symmetrical ketone, hereafter, is abbreviated as K*n*, where *n* is the number of carbon atoms, is different only from *n*-alkane, abbreviated as C*n*, in that the former has a carbonyl group with a permanent dipole moment at the center of the chain. They belong to the same crystal group for odd *n*, and the lattice constants of their sub-cells, which are orthorhombic, are almost the same. A characteristic difference in the thermal behavior between pure C*n* and K*n* crystals lies in that C*n* exhibits a couple of solid–solid phase transitions before melting, whereas K*n* melts without showing any solid–solid phase transition to the liquid phase at a temperature higher than the melting temperature of C*n* with the same *n*.[1–5] This difference has been attributed to rotational motion as well as sliding motion along the chain axis, which are allowed for C*n* chains, whereas the dipole–dipole interaction between the carbonyl groups is sufficiently strong enough for K*n* chains to hinder such molecular motions for induction of the phase transition.[6–10]

The forementioned similarity and difference between C*n* and K*n* crystals motivated us to construct phase diagrams of binary systems of C*n* and K*n* with different *n*. In previous reports,[11,12] where the DSC technique was exclusively employed, we determined phase diagrams for binary mixtures of C*n* and K*n* with the same or slightly different *n* ranging from 25 to 39 prepared by bulk-crystallization as well as solution-crystallization methods. Both methods gave essentially the same phase diagram for the K25/C25 system such that solid solutions are formed in a limited low range of the molar fraction (f_m) of K*n*, while above the solubility limit ($f_{m,c}$) eutectic mixtures are obtained.[11] On the other hand, different phase diagrams have been obtained for the K39/C39 system depending on the crystallization method used. The bulk-crystallized sample gave a phase diagram essentially the same as the K25/C25 system with a larger $f_{m,c}$ value, but the phase diagram for the solution-crystallized sample is quite complicated, as shown in Fig. 1, which has been reproduced from Ref. 13 for convenience of description in the Results and Discussion section. The most characteristic feature is that two different types of solid solutions are likely to be formed at room temperature over the entire range of f_m above and below $f_{m,c} = 0.204$. The phase diagram has been successfully reproduced in terms of the Flory–Huggins theory[14] with the phenomenological interaction parameter (χ_{12}) between C39 and K39 molecules, given by the solid curves in the figure. A positive χ_{12} value is necessary for data fitting, indicating that the enthalpy of mixing is positive to this system.

The vertical solid line of $f_{m,c} = 0.204$ in Fig. 1 distinguishes two solid solution regimes S_1 and S_2, and other two dashed lines in the S_1 regime are tentatively drawn referring to well-established results[11] for the solid–solid phase transitions of pure normal alkane C39 from the A phase of an orthorhombic crystal to the B phase of a monoclinic one and then to the C phase of more disordered monoclinic one. However, this assignment does not seem self-evident, since the solid–solid phase transition is usually observable only for a sufficiently pure sample and is rare for a binary mixture containing nearly 20 wt % of a minor component. Furthermore, we think that recrystallization must occur to form a K39-rich crystal in the liquid–solid solution coexistence region denoted as $S_2 + L$ in Fig. 1. Thus, it is likely that the phase diagram obtained from DSC measurements becomes more meaningful from a molecular point of view if crystal structures in respective phase could be definitely determined.

Published on the web July 11, 2007; doi:10.1246/bcsj.80.1316

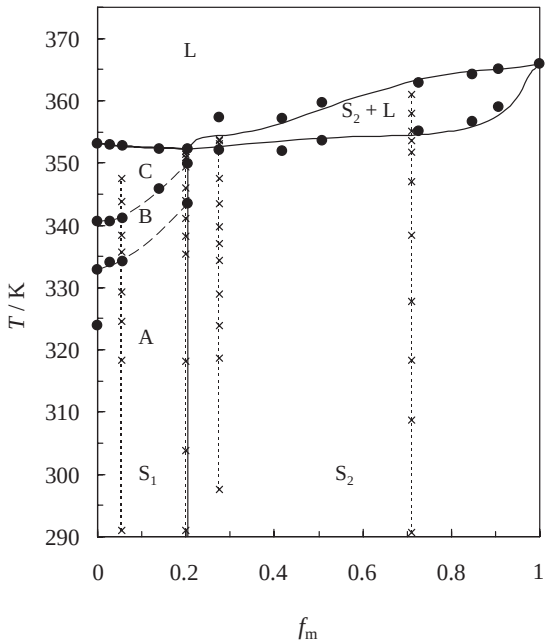

Fig. 1. Binary phase diagram for K39/C39 samples crystallized from toluene solution. Two different types of solid solutions (the regime S_1 and S_2) formed at room temperature over the entire range of f_m above and below $f_{m,c} = 0.204$, indicated as the vertical line. Solid lines were calculated in terms of the Flory–Huggins theory with the phenomenological interaction parameter χ_{12} between C39 and K39 molecules. X-ray diffraction measurements as a function of the temperature were performed on two pure samples, and four K39/C39 samples at elevated temperatures given by crosses.

In this paper, we performed X-ray diffraction measurements on twelve samples of the binary K39/C39 system including pure C39 and K39 at room temperature and also on four samples at elevated temperatures, given by crosses in Fig. 1, to determine the crystal structures in respective phases. Composition and temperature dependencies of a long period (L) and two subcell lengths (a_s and b_s) were studied in detail using (00ℓ), (200), and (110) reflection data, respectively. We found that the solid solutions in regime S_1 where $f_m < f_{m,c}$ had nearly the same crystal structure as that of pure C39, which is characteristic of two solid–solid phase transitions, while the crystal structures at room temperature in regime S_2 were dominantly affected by K39. In addition after the temperature was raised above the solidus line of the phase diagram, recrystallization occurred in the liquid–solid solution coexisting phase. The phase transition behavior to the C phase and resulting chain packing observed for samples with $f_m < f_{m,c}$ are discussed in relation to an intrachain defect effect as well as anomalous anisotropy of linear thermal expansion coefficients along two lattice directions.

Experimental

Materials. Symmetrical ketone 20-nonatriacontanone (K39) and the corresponding *n*-alkane C39 were used for this investigation. The ketone was synthesized through a ketene dimerization reaction from the corresponding carbonic acid chlorides, which were free from other homologues. Details of the purification technique of starting materials and the synthetic method are reported elsewhere.[15,16] K39 was finally purified with recrystallization and eluted through a silica column. C39 was synthesized by reducing the corresponding ketone K39 using the Wolff–Kishner method, and purified by using column chromatography after treatment with hot concentrated sulfuric acid. The sample purity was determined with a capillary gas chromatograph (GC-14A, Shimadzu) equipped with a column of CBP1-M25-025. The purity for homologues was up to 99.7% for both compounds.

After solubility tests of pure K39 and C39, using several organic solvents, we chose toluene as the solvent for solution-crystallization of K39/C39 binary system, because it is a good solvent for both of K39 and C39 and temperatures, at which crystallization took place, are located at around room temperature over the whole range of f_m of K39. Twelve samples including pure K39 and C39 samples were crystallized from 0.85% toluene solutions containing weighed amounts of K39 and C39 with a slow cooling rate of 0.02 to 0.05 K min^{-1}. The values of f_m of K39 in the binary crystals thus obtained were determined using the capillary gas chromatography, and were found to be close to mixing molar ratios of K39 in respective solutions, except at low f_m, where the former was much lower than the latter. A lozenge-shaped single crystal was obtained for pure C39 and K39, whereas the K39/C39 binary mixtures gave powder-like crystals, which became finer with increasing f_m.

Method. X-ray diffraction measurements were made on single crystal mats of pure C39 and K39 as well as powder-like crystals of K39/C39 binary system and of pure C39 and K39 with a Geiger flex 2027 diffractometer with Ni-filtered Cu Kα radiation (Rigaku). The samples were put inside a hollow of a 0.2 mm deep glass sample-plate and covered with a thin beryllium plate. The procedure provided accurate determination of L for the lozenge shaped single crystals due to high diffraction intensity of the (00ℓ) reflections, where even numbers of ℓ are observable because of the double layer structure characteristic of pure C39 and K39. The values of a_s and b_s were estimated from the (200) and (110) reflections at room temperature. Those quantities were also measured for four samples with $f_m = 0.0556$, 0.199, 0.276, and 0.71 from room temperature up to the respective melting temperatures by raising temperature successively as indicated in Fig. 1.

Results and Discussion

Composition Dependence of L, a_s, and b_s at Room Temperature. X-ray diffraction profiles at room temperature were essentially same for all samples tested and were characterized by peaks ascribed to (00ℓ), (200), and (110) reflections intrinsic of the orthorhombic type of crystal structure. Pure C39 and K39 as well as K39/C39 mixtures with low f_m gave a series of sharp (00ℓ) reflection peaks with high intensity. Peaks became broader with an increase in the f_m. Nevertheless, L was successfully determined as the intercept from linear extrapolation in a plot of $L(\ell)$ at various ℓ values against $1/\ell$, as shown in Fig. 2. In regime S_1 (Fig. 2a), the slope monotonously increased with increasing f_m, but linear extrapolation of the K39/C39 data with $f_m = 0.0556$, 0.139, and 0.199 gave L values in excellent agreement with the corresponding value for pure C39 ($L = 5.143$ nm). The latter agrees with that calculated from the empirical equation $L_{odd}/\text{nm} = 0.1267n + 0.2005$, reported by Urabe et al.[17] The slope for the sample with $f_{m,c} = 0.204$ that divides the two solid solution regimes appears surprisingly large. However, linear extrapolation gave

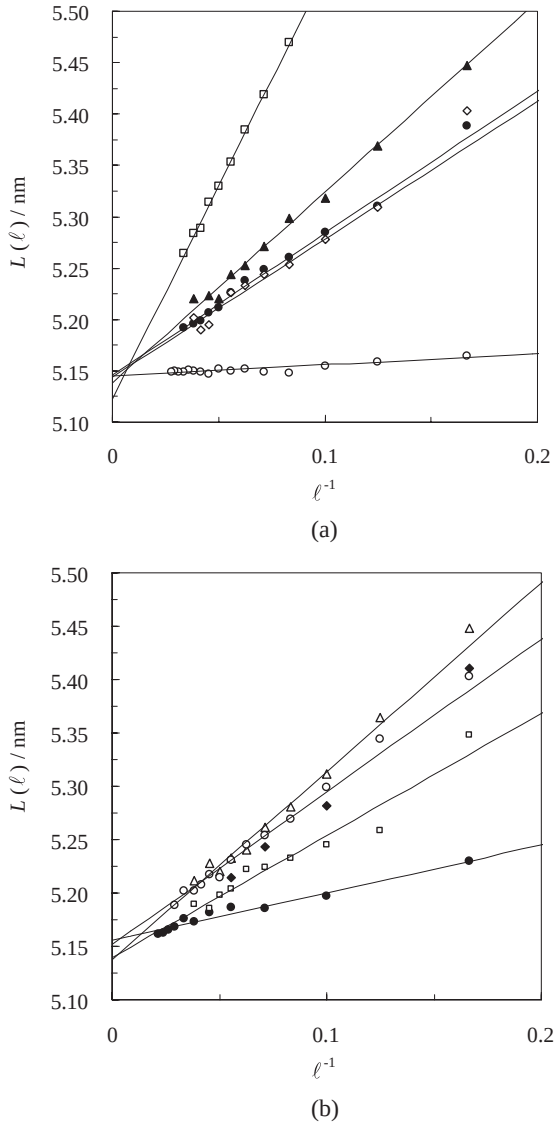

Fig. 2. L as the intercept from linear extrapolation in a plot of $L(\ell)$ at various Miller indices ℓ values against $1/\ell$. (a) Symbols are (○) pure C39, (◇) $f_m = 0.0556$, (●) $f_m = 0.139$, (▲) $f_m = 0.199$, and (□) $f_{m,c} = 0.204$. (b) Symbols are (△) $f_m = 0.276$, (○) $f_m = 0.419$, (□) $f_m = 0.509$, (◆) $f_m = 0.710$ and (●) pure K39.

a value slightly smaller than that for pure C39. In the S_2 regime above $f_{m,c}$, on the other hand, the slope starts to decrease with increasing f_m as shown in Fig. 2b. Occurrence of the maximum in the slope at $f_{m,c}$ suggests that severe distortion on layer stacking vertical to the main chain axis gives rise to two different regimes of solid solutions. Though scattering of data is considerably large in the S_2 regime, linearly extrapolated values agreed with the L value for pure K39 and also with that of pure C39, which confirms that the long period remains constant over the whole f_m range.

Figure 3 shows composition dependence of a_s and b_s at room temperature. As described in the Introduction, pure C39 and K39 form the subcell with the same size. a_s and b_s of solid solutions in the S_1 and the S_2 regimes are independent of f_m and are the same as those of the pure samples. Results on

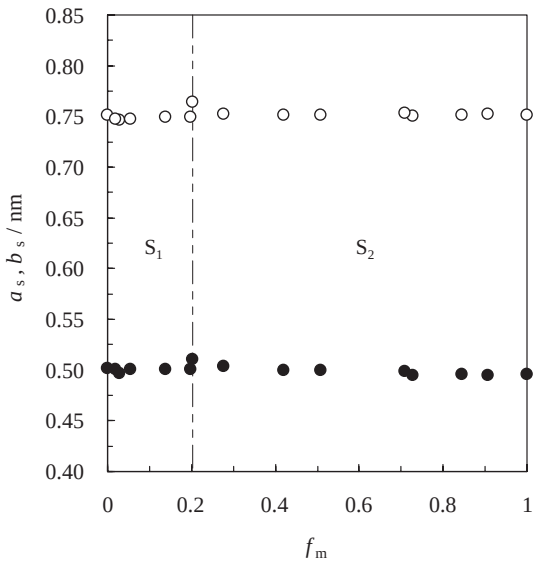

Fig. 3. Composition dependence of a_s (○) and b_s (●) at room temperature. The vertical broken line distinguishes two types of solid solutions in regime S_1 and S_2.

subcell dimensions demonstrate that solid solutions have an orthorhombic crystal structure same as either C39 or K39 at room temperature but cannot give information on differences in the crystal structure between the S_1 and the S_2 regime. Taking into account the phase diagram given in Fig. 1, we suppose that clear information shall be obtained from a study on the dependence of the lattice parameters on temperature.

Temperature Dependence of *L*. As is well known, C39 exhibits a solid–solid phase transition phenomenon that is affected by the delicate balance between the interfacial energy related to spatial alignment of end methyl groups and intermolecular interaction energy due to parallel alignment of trans zig-zag chains, whereas the strong dipole interaction of carbonyl groups between the double layer inhibits a solid–solid phase transition for K39 up to the melting point. Corresponding change of L with T is observed as shown in Fig. 4a, where the broken lines indicate the solid–solid phase transition temperatures detected as heat absorption peaks by DSC measurement for C39.[13] L of C39 appears to increase slightly through the $A' \rightarrow B$ phase transition and very sharply decreases due to the $B \rightarrow C$ phase transition. In the figure, the point given as the triangle is the calculated value of $L = 4.871$ nm assuming the M101 structure (Sullivan representation)[18,19] to the C39 crystal just before the melting point. The experimental appears to approach the point smoothly, which indicates that C39 gradually tilts, i.e., the high-temperature structure, in the C phase. On the other hand, L of K39 increased very gradually with the low thermal expansion coefficient as Fig. 4a shows.

Extrapolated L values of two K39/C39 samples with $f_m = 0.0556$ and 0.199 are plotted against absolute temperature T in Fig. 4b. Here, broken lines drawn vertically in the upper and the lower parts of the figure indicate the solid–solid phase transition temperatures for the samples with $f_m = 0.0556$ and 0.199, respectively, read from the phase diagram given in Fig. 1. A very small increase in L was observed in the B phase only for the sample with $f_m = 0.199$. However, a sharp de-

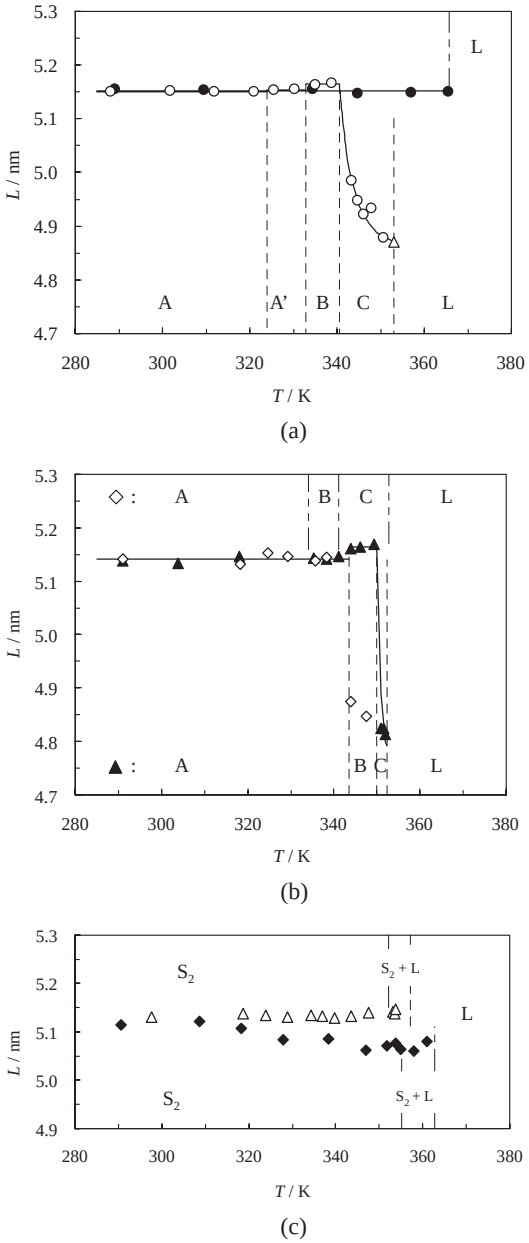

Fig. 4. (a) Temperature dependence of the extrapolated L of solution-crystallized samples of pure C39 (○) and pure K39 (●). The vertical broken lines indicate the solid–solid phase transition temperatures, and melting at 353 K for C39, respectively, and only melting at 366 K for K39 determined from DSC. Calculated value of L (4.871 nm), assuming the M101 structure for the C phase of C39, is plotted as the triangle (△). (b) Temperature dependence of the extrapolated L values of two samples in the S_1 regime with $f_m = 0.0556$ (◇) and $f_m = 0.199$ (▲). The broken lines drawn vertically in the upper and the lower parts of the figure indicate the solid–solid transition temperatures, respectively, read from the phase diagram given in Fig. 1. (c) Temperature dependence of the extrapolated L values of two samples belonging to the S_2 regime with $f_m = 0.276$ (△) and $f_m = 0.710$ (◆). The vertical broken lines indicate the transition temperatures, respectively, read from the phase diagram given in Fig. 1.

crease in L was observed for the both samples in a temperature region proposed as the C phase from DSC measurements following the well-established assignment on C39.

Figure 4c shows changes in L of two samples with $f_m = 0.276$ and 0.710 belonging to the S_2 regime as temperature was increased. These solid solutions are characterized by the presence of the liquid–solid solution coexistence phase, of which the temperature range is given by the broken lines in the figure. The diffraction intensities of all characteristic peaks started to decrease whenever temperature was raised into the coexistence region. Nevertheless, intensities remained sufficiently high enough for estimation of lattice parameters. This strongly suggests that recrystallization must occur in the coexistence phase so as to form a new crystal with higher molar fraction of the K39 component after melting of the original solid solution. The figure shows that L of the sample with $f_m = 0.276$ did not vary with T, while L of the sample with $f_m = 0.71$ gradually decreased with T in the solid solution phase but became constant in the coexistence phase. These results involving the temperature dependence of L reveal that there is a remarkable difference in the crystal structure between the solid solutions in the S_1 and the S_2 regimes.

Temperature Dependencies of a_s and b_s. Temperature dependence of a_s for pure C39 and for the two solid solutions with $f_m = 0.0556$ and 0.199 in the S_1 regime are plotted in Fig. 5a, where the broken lines drawn vertically in the upper and the lower parts of the figure indicate the solid–solid phase transition temperatures for C39 and the sample with $f_m = 0.199$, respectively. Corresponding temperatures for the sample with $f_m = 0.0556$ are close to those for C39 and are not shown for clarity of the figure. As is clear from the figure, a_s of the sample with $f_m = 0.0556$ closely followed the a_s vs. T curve of C39 empirically drawn and jumped about 0.007 nm (0.9%) at the B → C phase transition point. The increase in a_s of the sample with $f_m = 0.199$ with T was more gradual compared to that of C39 in the A phase, became sharper in the B phase, and then jumped at the B → C phase-transition point similar to that of C39. This behavior is in contrast to that in the S_2 regime shown in Fig. 5b. The a_s of K39 monotonously increased with T up to the melting temperature, and its linear thermal expansion coefficient along the a axis was lower than that of C39. The a_s of the sample with $f_m = 0.276$ closely followed the a_s vs. T curve of K39 empirically drawn before the coexistence phase, and then sharply increased up toward the a_s value of K39 at the melting point. The a_s of the sample with $f_m = 0.710$ was higher than that of K39, and through the phase transition from the solid solution phase to the coexistence phase once, decreased, followed by an increase, approaching the value of K39 at the melting point. The behaviors could be related to the occurrence of recrystallization in the coexistence phase.

Figures 6a and 6b show changes in b_s in the S_1 and S_2 regimes, respectively. In the S_1 regime, T dependence of b_s of the sample with $f_m = 0.0556$ is coincident with b_s of C39 in such way that b_s increased slightly with T in the A and B phases, and decreased in the C phase reaching a constant value finally. The b_s of the sample with $f_m = 0.199$ started to decrease in the B phase and more rapidly in the C phase. Changes in b_s with T in the S_2 regime were similar to those

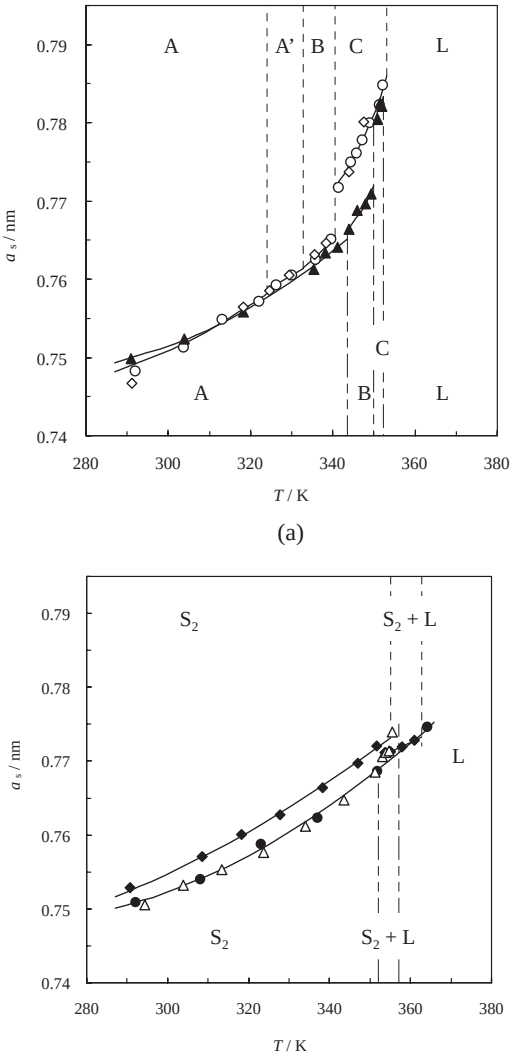

Fig. 5. (a) Temperature dependence of a_s for pure C39 (○) and for the two solid solutions with $f_m = 0.0556$ (◇) and $f_m = 0.199$ (▲) in the S_1 regime. Broken lines drawn vertically in the upper and the lower parts of the figure indicate the solid–solid phase transition temperatures for C39 and the sample with $f_m = 0.199$, respectively. Corresponding solid–solid phase transition temperatures for the sample with $f_m = 0.0556$ are close to those for C39. (b) Temperature dependence of a_s for pure K39 (●) and for the two samples in the S_2 regime with $f_m = 0.276$ (△) and $f_m = 0.710$ (◆) through the liquid–solid solution coexistence regime denoted as $S_2 + L$.

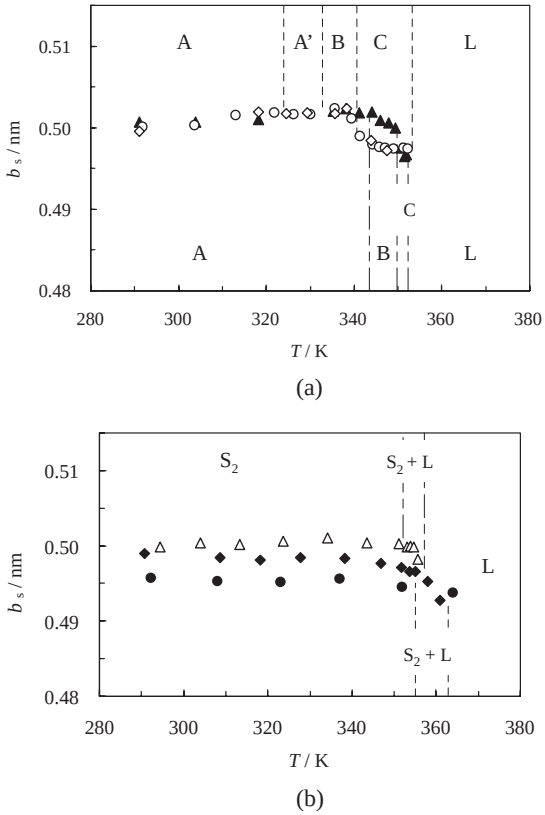

Fig. 6. (a) Temperature dependence of b_s for pure C39 (○) and two samples with $f_m = 0.0556$ (◇) and $f_m = 0.199$ (▲) in the S_1 regime. The phase notations are the same as in Fig. 5a. (b) Temperature dependence of b_s for pure K39 (●) and two samples with $f_m = 0.276$ (△) and $f_m = 0.710$ (◆) through the liquid–solid solution coexistence regime denoted as $S_2 + L$.

in the S_1 regime, however, the magnitude reflected the small difference of 0.005 nm in b_s between C39 and K39 at room temperature.

In summary, the study on temperature effects on three subcell parameters revealed that K39/C39 solid solutions can form two different orthorhombic crystal structures at room temperature. In the S_1 regime, the solid solutions exhibit two solid–solid phase transition phenomena with raising the temperature. Comparison with the behavior of C39 indicates that the solid solutions transform from the A structure to the B structure, and then to the C structure. The transition temperatures increased with an increase in the f_m of K39, which may be attributed to the dipole–dipole interaction of carbonyl residues. It seems remarkable that a similar crystal structure as that of pure C39 characteristic of three solid–solid phase transitions is maintained for the solid solutions with f_m up to a value of $f_{m,c}$ as large as 0.204, which is predicted from thermodynamic analysis using the Flory–Huggins theory in an earlier study.[13] We suspect that it is due to the small size of the carbonyl residues which can be accommodated inside the C39 crystal without severe perturbation as well as the use of very pure samples of C39 and K39 with $n = 39$ from a molecular point of view. In the S_2 regime, the solid–solid phase transition cannot occur before the samples melt, because the molecular motions along the main chain axis are inhibited due to the strong dipole–dipole interaction of carbonyl residues. Instead, the samples are likely to melt beyond the melting point of pure C39 crystal, which is accompanied by a large composition fluctuation or microscopic phase separation because of the positive interaction parameter estimated as $\chi_{12} = 1.5$ in a previous report.[13] As far as the temperature is lower than the melting point of pure K39, however, recrystallization may occur to form a solid solution very rich in the K39 component. This explains why the liquid–solid solution coexistence phase is ob-

served in the S_2 regime.

Solid–Solid Phase Transitions. The L of pure C39 determined from (00ℓ) reflections in the C phase is almost identical with that calculated for the M101 monoclinic structure, as shown in Fig. 4a. In microscope observations striations along the b axis on the surface of pure C39 single crystals after annealing were observed,[20,21] supporting the tilt transition reported earlier.[22–27]

The linear thermal expansion coefficients were determined from temperature dependence of a_s and b_s for the K39/C39 system. For the present, the solid–solid phase transition behaviors and resulting chain packing in the S_1 regime are discussed in relation to anomalous anisotropy of linear thermal expansion coefficients along two lattice directions. Generally speaking, the thermal expansions of the crystals depend on each lattice direction, and the coefficients of cubical expansions are approximated by the sum of each lattice direction. The anisotropy of linear thermal expansion coefficients for *n*-alkane homologues is due to an increase that is two times larger than Young's moduli.

First of all, we will examine the linear thermal expansion coefficients for each phase of C39, determined from the results of Figs. 5 and 6. The A phase (310–315 K) of an orthorhombic crystal had a linear thermal expansion coefficient along a_s direction of $41.3 \times 10^{-5}\,K^{-1}$, and that along b_s direction of $15.1 \times 10^{-5}\,K^{-1}$. These results imply the anisotropy of linear thermal expansion coefficients along two lattice directions is 2.7 times longer than b_s. The same behavior was observed in the B phase and C phase. The linear thermal expansion coefficient of the C phase along a_s direction was $152.3 \times 10^{-5}\,K^{-1}$ (345–351 K), similar to that of low molecular liquid state, and was 11 times greater than that along b_s. It is obvious that these results are the main cause of occurrence of freezing-in phenomena of high-temperature structures in the C phase.

Next, the linear thermal expansion coefficients of K39 were also examined. The value along a_s direction for the A phase was $33.9 \times 10^{-5}\,K^{-1}$ (310–315 K), while that along b_s direction was $-1.3 \times 10^{-5}\,K^{-1}$. Furthermore, the value along a_s of $54.1 \times 10^{-5}\,K^{-1}$ (345–350 K) and that along b_s of $-8.6 \times 10^{-5}\,K^{-1}$ were observed before melting. Although this temperature region corresponds to that of C phase for C39, a small change in the value along a_s was obtained.

These results for K39 agree with those obtained for C39 so that two crystals have the same anisotropy of linear thermal expansion coefficients. It seems reasonable that the effects of dipole–dipole interactions between carbonyl residues make the aggregation force for pure K39 chains strong.

The linear thermal expansion coefficients in the S_1 regime were also examined. The values along a_s direction for $f_m = 0.199$ near $f_{m,c}$ were $35.1 \times 10^{-5}\,K^{-1}$ in the A phase, $111.2 \times 10^{-5}\,K^{-1}$ in the B phase, and $173.7 \times 10^{-5}\,K^{-1}$ in the C phase, respectively, and increased as T approached the melting point. On the other hand, the value along b_s decreased. It is likely that thermal behavior in the S_1 regime is dominantly affected by pure C39.

The linear thermal expansion coefficients in the S_2 regime were also examined. The results of both $f_m = 0.276$ and $f_m = 0.710$ were almost the same as that of K39 as stated above.

Furthermore, the temperature changes for the products of a_s and b_s, that is, the *ab* planes in the S_1 regime, were examined. Discontinuous increases of the *ab* are observed in the B → C phase transition. It is likely that the increase of molecular motion along the *c* axis resulted in the oblique structures.

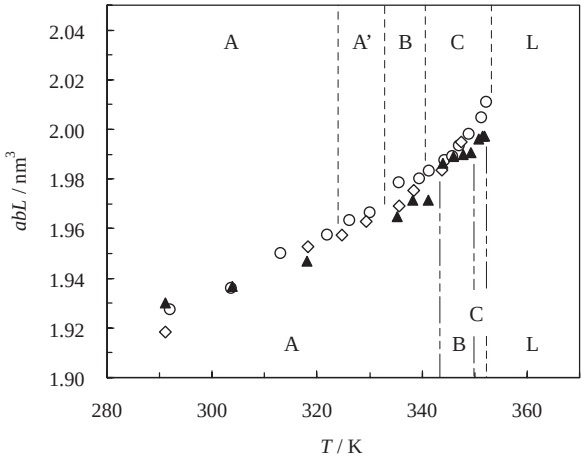

Fig. 7. Temperature dependence of *abL* for pure C39 (○) and two samples in the S_1 regime with $f_m = 0.0556$ (◇) and $f_m = 0.199$ (▲). The phase notations are the same as in Fig. 5a.

The half volume of a unit cell in the regime S_1 (*abL*) is plotted as a function of temperature in Fig. 7. The *abL* of C39 (○) slightly increased at the B → C phase transition point and also in the C phase. On the other hand, the *abL* of $f_m = 0.0556$ (◇) and $f_m = 0.199$ (▲) increased discontinuously in the same transitions. The volume change for pure C39 crystal was slightly higher than those of other crystals in the regime S_1. It is clear that the effect of dipole–dipole interaction induces the rapid tilt formation in the C phase on the binary system.

Concluding Remarks

In this study, X-ray diffraction measurements were made on single crystal mats of the K39/C39 binary system crystallized from the solution, and we determined the crystal structures in the respective phases of the phase diagram obtained from DSC. In the phase diagram of K39/C39 system, two different types of solid solutions (the regime S_1 and S_2) above and below $f_{m,c} = 0.204$ formed.

Composition and temperature dependencies of L and a_s and b_s were studied in detail using (00ℓ), (200), and (110) reflection data. We found that the solid solutions in the regime S_1 of $f_m < f_{m,c}$ had the same crystal structure as that of pure C39 characteristic of two solid–solid phase transitions. Furthermore, it was found that the B → C phase transition for the regime S_1 occurred more rapidly than that of pure C39. These phase-transition behaviors and resulting chain packing were discussed in relation to anomalous anisotropy of linear thermal expansion coefficients along a_s and b_s lattice directions.

On the other hand, the crystal structures at room temperature in the regime S_2 were affected by K39. After temperature was raised above the solidus line of the phase diagram, recrystallization occurred in the liquid–solid solution coexistence phase. These results from X-ray measurements are consistent with the phase diagram determined from DSC.

References

1 W. B. Saville, G. Shearer, *J. Chem. Soc.* **1925**, *127*, 591.
2 A. Müller, W. B. Saville, *J. Chem. Soc.* **1925**, *127*, 599.
3 S. H. Piper, A. C. Chibnall, S. J. Hopkins, A. Pollard, J. Andrew, B. Smith, B. F. Williams, *Biochem. J.* **1931**, *25*, 2072.
4 J. W. H. Oldham, A. R. Ubbelohde, *Trans. Faraday Soc.* **1939**, *35*, 328.
5 K. Nakasone, Y. Urabe, K. Takamizawa, *Thermochim. Acta* **1996**, *286*, 161.
6 J. W. H. Oldham, A. R. Ubbelohde, *Proc. Roy. Soc. A* **1940**, *176*, 50.
7 R. J. Meakins, *Aust. J. Sci. Res.* **1949**, *2*, 405.
8 R. J. Meakins, *Trans. Faraday Soc.* **1959**, *55*, 1964.
9 R. J. Meakins, *Trans. Faraday Soc.* **1959**, *55*, 1702.
10 R. G. Strobl, T. Trezebiatowski, B. Ewen, *Prog. Colloid Polym. Sci.* **1978**, *64*, 219.
11 K. Takamizawa, K. Nakasone, Y. Urabe, *Colloid Polym. Sci.* **1994**, *272*, 293.
12 K. Takamizawa, K. Nakasone, Y. Urabe, T. Sonoda, *Eng. Sci. Rep., Kyushu Univ.* **1990**, *12*, 291.
13 K. Nakasone, K. Shiokawa, Y. Urabe, N. Nemoto, *J. Phys. Chem. B* **2000**, *104*, 7483.
14 P. J. Flory, *Principles of Polymer Chemistry*, Cornell Univ. Press, Ithaca, **1953**.
15 K. Takamizawa, T. Sonoda, Y. Urabe, *Eng. Sci. Rep., Kyushu Univ.* **1989**, *10*, 363.
16 K. Nakasone, *Bull. Coll. Sci., Univ. Ryukyus* **1996**, *62*, 1.
17 Y. Urabe, M. Saito, H. Fujiwara, N. Nemoto, *Technol. Rep. Kyushu Univ.* **1999**, *72*, 101.
18 P. K. Sullivan, J. J. Weeks, *J. Res. Natl. Bur. Stand., Sect. A* **1970**, *74*, 203.
19 P. K. Sullivan, *J. Res. Natl. Bur. Stand., Sect. A* **1974**, *78*, 129.
20 K. Takamizawa, Y. Urabe, J. Fujimoto, H. Ogata, Y. Ogawa, *Thermochim. Acta* **1995**, *267*, 297.
21 K. Nakasone, K. Takamizawa, K. Shiokawa, Y. Urabe, *Thermochim. Acta* **1994**, *233*, 175.
22 W. Piesczek, G. R. Strobl, K. Malzahn, *Acta Crystallogr., Sect. B* **1974**, *30*, 1278.
23 G. Strobl, B. Ewen, E. W. Fischer, W. Piesczek, *J. Chem. Phys.* **1974**, *61*, 5257.
24 B. Ewen, G. R. Strobl, D. Richter, *Faraday Discuss.* **1980**, *69*, 19.
25 K. Takamizawa, Y. Ogawa, T. Oyama, *Polym. J.* **1982**, *14*, 441.
26 G. Ungar, X. B. Zeng, *Chem. Rev.* **2001**, *101*, 4157.
27 D. S. M. de Silva, X.-b. Zeng, G. Ungar, S. J. Spells, *Macromolecules* **2002**, *35*, 7730.